bioRxiv preprint doi: https://doi.org/10.1101/2024.02.21.581353; this version posted February 23, 2024. The copyright holder for this preprint (which was not certified by peer review) is the author/funder, who has granted bioRxiv a license to display the preprint in perpetuity. It is made available under aCC-BY-NC-ND 4.0 International license.

Title: Radiation-induced non-neoplastic cells senescence promoting the proliferation and invasiveness of GBM through SASP/JAK2-STAT3 Pathway

Running title: Senescent microenvironment promotes proliferation and invasion of GBM

Authors: Pan Nie[1,2] M.D., Jincao Chen[1,2#] M.D., Ph.D., Prof., Jibo Zhang[1,2#] M.D., Ph.D..

# These authors are co-corresponding authors.

Affiliations:

[1.] Department of Neurosurgery, Zhongnan Hospital of Wuhan University, Wuhan 430071, China.

2. Brain Research Center, Zhongnan Hospital of Wuhan University, Wuhan, China.

Corresponding Author:

Jibo Zhang M.D., Ph.D.

Department of Neurosurgery

Zhongnan Hospital of Wuhan University

Donghu Road 169, Wuhan 430071, China

Tel: 13349908832

FAX: +86-27-67812892

e-mail: zhangjibo0007@163.com

Jincao Chen M.D., Ph.D., Prof.

Department of Neurosurgery

Zhongnan Hospital of Wuhan University

Donghu Road 169, Wuhan 430071, China

Tel: +86-27-67813236 (office), +86-13971091714(mobile)

FAX: +86-27-67812892

e-mail: chenjincao88@163.com

bioRxiv preprint doi: https://doi.org/10.1101/2024.02.21.581353; this version posted February 23, 2024. The copyright holder for this preprint (which was not certified by peer review) is the author/funder, who has granted bioRxiv a license to display the preprint in perpetuity. It is made available under aCC-BY-NC-ND 4.0 International license.

Abstract

Objective: To investigate the impact of radiation-induced senescent tumor microenvironment on the proliferation and aggressiveness of GBM, as well as its underlying mechanism.

Methods: Pre-irradiate astrocytes or mice for the in vitro and in vivo establishment of senescent environments. Simulate the impact of the senescent microenvironment on GBM by treating tumor cells with conditioned medium and utilizing a xenograft tumor model, followed by observation and documentation of the biological characteristics of tumor cells and survival time of mice. The anti-senescence drug was used to eliminate senescent cells in the brain of mice after radiation.

Results: Astrocytes can be obviously stained by β-galactosidase staining after exposed to X-ray, and the expression of P16 and P21 genes is significantly upregulated. Cell viability assay, transwell invasion assay and wound healing assay demonstrated that GBM cells treated with senescence medium exhibited enhanced proliferation, increased migration and invasion capabilities compared to those treated with normal medium. Irradiated mice displayed larger tumor volume 20 days after tumor implantation and shorter survival times than mice in control group. Administration of navitoclax reduced tumor volume and extended survival time in mice. The transcriptome sequencing and protein detection identified IL6 as the exclusive highly expressed senescence secretion phenotype in senescence medium, which activates the JAK2-STAT3 signaling pathway in tumor cells.

Conclusion: The tumor microenvironment, consisting of non-neoplastic cell senescence induced by radiotherapy and its secretory phenotype, can facilitate the proliferation and invasion of GBM, indicating the favorable role of senescent cells in the recurrence of residual GBM. This process is mediated through the activation of JAK2-STAT3 signaling pathway by SASP factor IL6. Anti-senescence drugs may emerge as a novel adjunctive therapeutic approach to delay GBM recurrence.

Key words: Glioblastoma, Radiotherapy, Senescent cell, Senescence-associated secretory phenotype, IL6

Background

bioRxiv preprint doi: https://doi.org/10.1101/2024.02.21.581353; this version posted February 23, 2024. The copyright holder for this preprint (which was not certified by peer review) is the author/funder, who has granted bioRxiv a license to display the preprint in perpetuity. It is made available under aCC-BY-NC-ND 4.0 International license.

Glioblastoma (GBM) is an extremely aggressive and malignant brain tumor in the central nervous system, presenting significant treatment challenges due to its rapid growth, invasive nature, and resistance to conventional therapies[1, 2]. Despite aggressive management involving maximal safe surgical resection followed by radiation therapy (60 Gy/30 fractions) with concomitant and adjuvant temozolomide, patients inevitably experience disease recurrence, with a median progression-free survival of less than 2 years[3, 4].

Explanations for GBM recurrence and improved treatment strategies may necessitate a more profound understanding of radiation-induced alterations in the tumor microenvironment. Radiation can directly impact the structure of the DNA double helix, and subsequently activating DNA damage sensors to induce apoptosis, necrosis and senescence[5]. Consequently, it is common to observe rapid tumor volume reduction during early stages of radiation therapy. However, subsequent recurrent tumors frequently emerge within the irradiation range, exhibiting accelerated growth, heightened aggressiveness and resistance to treatment[1, 6-9]. Presumably, specific alterations induced by radiation within the tumor microenvironment may contribute to GBM recurrence while conferring higher aggressiveness and treatment resistance[9]. We propose that radiation-induces senescence in non-neoplastic brain cells within the tumor microenvironment facilitates GBM recurrence.

Cell senescence is a highly heterogeneous state of growth arrest characterized by resistance to apoptotic stimuli and increased secretion of chemokines, cytokines, and growth factors[10]. The stability of the cell cycle arrest relies on the cyclin-dependent kinase (CDK) inhibitors p16 and p21 and whose elevated expression serves as a marker for senescence detection[11]. Another important feature of senescent cells is upregulation of the lysosomal enzyme β-galactosidase activity, which can be visualized using β-galactosidase staining and is commonly used for detecting senescent cells[12]. Senescent cells secrete growth factors, interleukins, extracellular matrix (ECM) components, and ECM-modifying metalloproteases that together create a complex and variable senescence-associated secretory phenotype (SASP)[13, 14]. Studies have shown that stromal cells senescence can promote the growth of tumor cells in breast, lung, liver, and skin cancer through SASP[15, 16]. Radiation has been found to induce senescence in astrocytes with a predisposition to undergo this process[17]. Therefore, exploring the tumor-promoting potential and mechanisms of radiation-induced non-neoplastic cell senescence and its associated secretory phenotype in GBM is warranted. Using in vitro induced senescent cell models and xenografted orthotopic tumor mice models, We demonstrated that irradiation-induced senescence of non-neoplastic cells promotes proliferation and invasion of GBM cells via activation of JAK2-STAT3 signaling pathway by the secreted SASP factor IL6. Importantly, we show that this detrimental effect can be mitigated by administration of navitoclax—an anti-senescence drug—providing a novel adjunctive therapeutic approach for delaying and treating GBM

bioRxiv preprint doi: https://doi.org/10.1101/2024.02.21.581353; this version posted February 23, 2024. The copyright holder for this preprint (which was not certified by peer review) is the author/funder, who has granted bioRxiv a license to display the preprint in perpetuity. It is made available under aCC-BY-NC-ND 4.0 International license.

recurrence.

Materials and Methods

Radiation induced astrocytes senescence

Normal Human Astrocyte (NHA) cell line were purchased from the Chinese Academy of Sciences Typical Culture Preservation Committee Cell Bank (CAS Shanghai Cell Bank) and cultured in H-DMEM (Servicebio, G4511) medium containing 10% fetal bovine serum (FBS, PAN Seratech, ST30-3302) and 1% streptomycin mixture (100X, Servicebio, GP2308019) at 37°C in a constant-temperature incubator with 5% CO_2. NHA cells were induced to senescence by irradiation with a dose of 10 Gy using an X-Ray irradiator (X-RAD 320, Precision X-ray) when the cells reached approximately 100% confluence in 10cm petri dish. Control cells were mock-irradiated. The senescence phenotype was detected through β-galactosidase staining and analysis of P16 and P21 gene expression at day 7 post-irradiation, during which the medium was changed twice. At day 8 post-irradiation, after incubating the cells for 24 hours with serum-free media, the medium from both irradiated (conditional medium, CM) and non-irradiated (normal medium, NM) cells was harvested. The medium was filtered with a 40um cell filter, followed by centrifugation at 1000×g for 20 minutes to collect the supernatant (Fig 1). Finally, the complete medium was prepared by supplementing the supernatant with 10% fetal bovine serum.

Senescence-associated β-galactosidase staining

The experiment was conducted following the protocol of β-galactosidase staining kit (Solarbio, G1580). Cell staining was performed according to the adherent cell staining protocol. Briefly, cells were washed with PBS and fixed at room temperature with β-Gal fixing solution (1ml/ well in 6-well plate) for 15 minutes. The fixing solution was then removed and cells were washed again with PBS three times. Subsequently, the dyeing working solution (1ml/well in the 6-well plate) was added and cells were incubated overnight in a non-carbon dioxide incubator at 37℃. Observation made using an ordinary optical microscopy. Tissue section staining followed the frozen section staining protocol which included similar processes as cell staining: washing, fixing, washing, staining and observation. ImageJ software was used for senescent cell counting.

Cell Viability Assay

The proliferation capacity of human GBM cell lines U251(Procell, CL-0237) and A172(Procell, CL-0012) cultured in CM and NM was evaluated by CCK-8 assay. The experiment followed the CCK-8 kit (YEASEN,C8102040) protocol. Cells were seeded at a density of 5×10^3 cells per well in a 96-well plate and incubated in different media for 3 days. The cell viability was assessed at 24-hour intervals until the culture wells were fully populated. For detection, 10 μl of CCK-8 reagent was added to each well and incubated at 37℃ for 2 hours. Subsequently, the absorbance at

bioRxiv preprint doi: https://doi.org/10.1101/2024.02.21.581353; this version posted February 23, 2024. The copyright holder for this preprint (which was not certified by peer review) is the author/funder, who has granted bioRxiv a license to display the preprint in perpetuity. It is made available under aCC-BY-NC-ND 4.0 International license.

450 nm was measured using a spectrophotometer.

Transwell Invasion Assay

The invasion ability of U251 cells and A172 cells was evaluated through transwell invasion assay. Matrigel was melted at 4℃ and diluted to a concentration of 1 mg/mL in culture medium without FBS one day prior to use. CM and NM were separately added into the lower chamber of the 24-well transwell plate. Subsequently, 100 μL of matrigel (1mg/mL) was added into the upper chamber and incubated for 4h until it polymerized. Then, U251 cells and A172 cells were seeded into the upper chamber at a density of 2×10^5 cells per well in 200 μL of serum-free medium. The culture system was then incubated for 24 hours in an incubator. Cells were fixed with 4% paraformaldehyde for 2 minutes, permeabilized with 100% methanol for 20 min, and stained with Wright's Giemsa solution for 15 minutes at room temperature. The stained cells were imaged via microscopy.

Wound Healing Assay

The migration ability of U251 cells and A172 cells in CM and NM was evaluated by Wound Healing Assay. Cells were seeded at a density of 5×10^5 cells per well in six-well plates. Subsequently, three scratches were made on the monolayer of cells using a 200-μL sterile pipette tip, and cells were washed thrice with PBS to eliminate cellular debris. To ensure the uniformity of each scratch, the cells were initially observed under a microscope at 0 h as the control condition. Finally, the treated cells were observed and imaged via microscopy, and the migration distance was calculated using ImageJ software.

Immunofluorescence staining

The expression of ki67 protein in U251 cells treated with different media was detected through immunofluorescence staining to evaluate the cellular proliferation capacity. A circular slide was placed inside a 6-well plate and sterilized under ultraviolet light for 30 minutes before inoculating U251 cells into the plate. After one week of culture in the two mediums, the slides covered with cells were removed and utilized for immunofluorescence staining. Cells were washed three times with PBS at 4℃, fixed with 4% paraformaldehyde for 15 min, and then immersed three times (5 min each time) in PBS containing 0.1% TritonX-100. Subsequently, the cells were incubated overnight at 4℃ in a wet box with ki67 primary antibody (Servicebio, GB111141), followed by incubation with a fluorescent secondary antibody (Fitc-labeled Goat Anti-Rabbit IgG, Servicebio, GB22303) for 1 hour. After dark staining with DAPI (Servicebio, GDP1024) for 3 minutes, samples were incubated with an antifade mounting medium and coverslipped accordingly. ki67 proteins were labeled with green fluorescence, while DAPI was labeled with blue fluorescence.

bioRxiv preprint doi: https://doi.org/10.1101/2024.02.21.581353; this version posted February 23, 2024. The copyright holder for this preprint (which was not certified by peer review) is the author/funder, who has granted bioRxiv a license to display the preprint in perpetuity. It is made available under aCC-BY-NC-ND 4.0 International license.

RNA extraction and qRT-PCR

We extracted total RNA from irradiated and non-irradiated NHA cells and from conditioned medium treated U251 and A172 cells. RNA was extracted by RNAiso Plus (Takara, No.9109) according to the manufacturer's instructions. Add 50ul of enzyme-free water and measure the RNA concentration (IMPLEN, NanoPhotometer N50). cDNA synthesis was performed using HiScriptⅣRT SuperMix for qPCR (Vazyme, R423-00) following the manufacturer's instructions. Quantitative PCR was performed to analyze gene expression using 2*ChamQ Universal SYBR (Vazyme, Q711-02) according to the manufacturer's instructions. All samples were amplified in bipartite. Measurements were standardized to GAPDH housekeeping gene.

RNA-seq of NHA and U251

RNA samples from cells are subject to rigorous quality control through Agilent 2100 bioanalyzer: Accurate detection of RNA integrity. All samples showed RNA integrity of >7.5. RNA-seq libraries were prepared using the NEBNext Ultra II RNA Library Prep Kit for Illumina (New England Biolabs, no. E7775) according to the manufacturer's instructions. After the library inspection is qualified, different libraries are carried out Illumina sequencing after pooling according to the effective concentration and requirements of target data volume. Image data from high-throughput sequencers were converted into sequence data (reads) by CASAVA base recognition. The index of the reference genome was constructed using HISAT2 v2.0.5, and the paired end clean reads were compared with the reference genome using HISAT2 v2.0.5. FeatureCounts (1.5.0-p3) is used to quantify gene expression levels.The DESeq2 software (1.20.0) was used for differential expression analysis between the two comparison combinations. Statistical enrichment of differentially expressed genes in the KEGG pathway was analyzed using clusterProfiler (3.4.4) software.

Protein extraction and Western blotting

Western blotting (WB) was performed to detect p-JAK2(Cell signaling: JAK2, 3230T; p-JAK2, 4406T) and p-STAT3(Cell signaling: STAT3, 9139T; p-STAT3, 9145T) proteins activated by IL6 in U251 cells after treated by CM. Briefly, proteins were extracted from cells using RIPA lysis buffer (Servicebio, G2002) supplemented with PMSF (Servicebio, G2008) and a phosphatase inhibitor (Servicebio, G2007), and protein levels were quantified using a BCA protein assay kit (Beyotime, P0009) according to the manufacturer's instructions. The proteins were then separated by 10% SDS-PAGE gels and transferred onto PVDF membranes. After blocking with fastest sealing fluid (HYCEZMBIO, HYC00811) at room temperature for 1 hour, the membranes were incubated with primary and secondary antibodies before being soaked in enhanced. Finally, membranes were soaked in enhanced ECL reagents (Servicebio, G2014) and protein bands were detected using a UVP BioSpectrum Imaging System. The intensities of protein bands were quantified with ImageJ software.

bioRxiv preprint doi: https://doi.org/10.1101/2024.02.21.581353; this version posted February 23, 2024. The copyright holder for this preprint (which was not certified by peer review) is the author/funder, who has granted bioRxiv a license to display the preprint in perpetuity. It is made available under aCC-BY-NC-ND 4.0 International license.

ELISA

The SASP factors with significant differences in qRT-PCR results were quantitatively detected in culture medium, including IL6 (ELK biotechnology, ELK1156), IL1b (ELK biotechnology, ELK1270), MMP1 (ELK biotechnology, ELK2183), FGF2 (ELK biotechnology, ELK1258), CXCL2 (ELK biotechnology, ELK2079). The experiments followed the kits protocols. The absorbance measured at a wavelength of 450 nm using the standard substance concentration was utilized to generate the curve. The concentrations of the unknown samples were subsequently determined from the absorbance curve by employing the slope and intercept obtained from it.

Tissue frozen section

The brain samples of mice and GBM samples from patients (Department of Neurosurgery, Zhongnan Hospital, Wuhan University) were processed into frozen sections for subsequent staining. After washing with PBS, the GBM samples was fixed in 4% paraformaldehyde for 24 hours, followed by dehydration in 20% sucrose solution for 48 hours. Mice were perfused with 4% paraformaldehyde and their brains were dissected out, then fixed and dehydrated as previously described. The tissue was embedded in O.C.T. compound (SAKURA, 4583) and frozen in the cryostat microtome (RWD, Minux FS800). Once both the embedding agent and the tissue had completely frozen to a white ice state, the tissue could be sliced into sections at a thickness of 20 micrometers. The sections were stained with hematoxylin and eosin (H&E; 0.1–0.5%). Finally, we observed and imaged the stained sections under an inverted microscope.

Animal studies

BALB/c nude mice (6–8 weeks in age, female) were purchased from Wanqian Jiahe Experimental Animal Farm in Wuhan, which are immune-deficient mice without thymus and can be implanted with xenogenic tumors. Cranial irradiation was performed using an X-ray device (X-RAD 320, Precision X-ray), with the mice placed in a lead box that exposed only their brains. To prevent oral mucositis, which has been observed in C57BL/6J mice when directly irradiated on the tongue with higher doses, the radiotherapy dose was limited to 10 Gy[18]. Control mice underwent anesthesia and sham irradiation. In order to investigate the development and temporal changes of radiation-induced senescent cells in the brain of live mice, the brains of irradiated mice at different time points (0d, 2d, 7d, 14d, 21d, 28d ,35d ,42d ,49d) were dissected and stained with β -galactosidase. Senescent cells were quantified using ImageJ software.

The U251 tumor cells (300,000 per mouse) were implanted into the right striatum of mouse brain 48 hours after irradiation. Daily observations were made on the mice's condition and weight. At day 20 post-implantation, an enhanced CT scan was performed to measure tumor size in the mouse brain. Mice were killed when they met near-death or humanitarian endpoints, including

bioRxiv preprint doi: https://doi.org/10.1101/2024.02.21.581353; this version posted February 23, 2024. The copyright holder for this preprint (which was not certified by peer review) is the author/funder, who has granted bioRxiv a license to display the preprint in perpetuity. It is made available under aCC-BY-NC-ND 4.0 International license.

hunchback and lethargy, seizures, and weight loss exceeding 20 percent. To investigate the impact of radiation-induced senescent cells on tumor growth, mice received daily oral gavage of anti-senescence drug navitoclax (Shanghai yuanye Bio-Technology Co., Ltd, S81105) at a dose of 50 mg/kg in corn oil starting 24 hours after cranial irradiation for a minimum duration of 25 days. The control group received vehicle alone. All animal studies were performed under protocols approved by Experimental animal Welfare Ethics Committee, Zhongnan Hospital of Wuhan University (ZN2022179).

Enhanced CT on brain of mice

In order to assess the growth of the orthotopic xenograft tumor in the mouse brain, an enhanced CT scan of the mouse brain was conducted on the 20th day post-implantation, enabling acquisition of a three-dimensional image and real-time volume measurement of the tumor. The CT equipment used for this study was NEMO Micro CT (NMC-200) manufactured by PINGSENG Healthcare Kunshan Inc. Prior to imaging, mice were anesthetized with 1% pentobarbital sodium and administered a tail vein injection of 300ul iopanol solution. Subsequently, mice were promptly positioned prone on a CT bed equipped with a nose cone for continuous anesthesia using isoflurane. Image acquisition software called Cruiser (PINGSENG Healthcare Kunshan Inc) facilitated capturing images according to a predefined scanning program in approximately 6 minutes. Post-processing of acquired images was performed using Avatar software (PINGSENG Healthcare Kunshan Inc).

Statistics

Statistical analyses were performed by using independent-samples t-test with GraphPad Prism (GraphPad 8 Software). Data were expressed as mean ± SD. Kapla-Meier functions were used to illustrate survival profiles of mice.Statistical significance was defined as $P < 0.05$.

Results

Radiation induced cellular senescence

In this study, we confirmed the occurrence of radiation-induced senescence in astrocytes. The identification of cellular senescence primarily relied on β-galactosidase staining and the expression analysis of P21 and p16 genes. NHA cells were subjected to β-galactosidase staining 7 days after exposure to a dose of 10Gy irradiation or mock-irradiation. Following irradiation, almost all the cells exhibited evident staining, while those in the mock-irradiation group remained largely unstained (Fig2, A). Furthermore, NHA cells displayed significant higher levels of P21 and P16 gene expression post-radiation treatment than mock-irradiation (Fig2, B). To investigate the duration of radiation-induced cellular senescence in mouse brains, we assessed and quantified senescent cells at various time points following irradiation. The results revealed that the number of

bioRxiv preprint doi: https://doi.org/10.1101/2024.02.21.581353; this version posted February 23, 2024. The copyright holder for this preprint (which was not certified by peer review) is the author/funder, who has granted bioRxiv a license to display the preprint in perpetuity. It is made available under aCC-BY-NC-ND 4.0 International license.

senescent cells peaked between 2 to 7 days after irradiation before gradually declining, and the number of senescent cells was still higher than that of non-irradiated mice at 49 days (Fig2, C, D). In addition, we conducted further assessment of cellular senescence in human GBM specimens and observed a significantly higher presence of senescent cells in recurrent tumors (all of which underwent complete radiation therapy) compared to primary tumors (Fig2, E).

Senescent astrocyte culture medium promotes tumor proliferation and invasiveness

We administered astrocytes with a dosage equivalent to that used in animal experiments and obtained conditioned media to mimic the tumor microenvironment consisting of senescent cells and their secretory phenotypes. The conditioned medium (as described above), which contains SASP, was collected on day 8 post-irradiation. U251 cells and A172 cells were treated with CM or NM. CCK-8 assay revealed that GBM cells exhibited faster proliferation rate following treatment with CM (Fig3, A, B). Correspondingly, both RNA and protein levels in tumor cells showed increased ki67 expression in CM group (Fig3, C, D). Furthermore, wound healing assays and transwell invasion assays were employed to assess migration and invasion abilities of tumor cells, yielding similar results: scratches were repaired more rapidly in CM group (Fig3, E, F, G), while more cells migrated through matrigel and pores in transwell upper chamber compared to those in NM group (Fig3, H).

Radiation induced senescent microenvironment can promote GBM proliferation

In order to mitigate immune rejection of human tumor cells in mice, immunodeficient BABLc-nude mice were selected. Anti-senescence drugs were administered to eliminate senescent cells in the brains of mice. Based on different treatment methods, the mice were divided into four groups: control group, radiation group, radiation combined dose group, and dose group. At 20 days post-tumor implantation, enhanced CT was utilized to measure tumor size in each group and late software processing was employed to present the three-dimensional shape of the tumor for understanding tumor spread and predicting aggressiveness. Additionally, the survival time of the mice was recorded. Enhanced CT at 20 days after implantation revealed that tumors volume in the radiation group measured 76.0 ± 31.4 mm^3 compared to 26.8 ± 14.2 mm^3 in the control group (Fig4,A,C;Table1). Notably, the tumor volume in the radiation combined dose group (38.3 ± 16.5 mm^3) was significantly smaller than that of the radiation group (Fig4,A,C;Table1). Three-dimensional reconstructions of the tumors showed the most irregular shape in the radiation group, potentially indicating a more aggressive nature. This observation was further confirmed through H&E staining, where an indistinct boundary between the tumor and normal brain tissue was observed alongside increased necrosis and angiogenesis within the tumor tissue in the radiation group (Fig4, B). Survival analysis demonstrated that survival time for mice in the radiation group (22.3 ± 1.7 days) was significantly shorter than that recorded for control group (26.7 ± 3.1 days; Fig4, F; Table1). Furthermore, survival time was prolonged in the radiation

bioRxiv preprint doi: https://doi.org/10.1101/2024.02.21.581353; this version posted February 23, 2024. The copyright holder for this preprint (which was not certified by peer review) is the author/funder, who has granted bioRxiv a license to display the preprint in perpetuity. It is made available under aCC-BY-NC-ND 4.0 International license.

combined dose group(27.1±3.3 days) compared with radiation group(Fig4, G; Table1). However, no significant prolongation of survival time occurred when comparing dose group with control group (Fig4, E; Table1).

Senescent cell secretory factor IL6 activates JAK2-STAT3 pathway in GBM cells

We performed transcriptome sequencing of NHA cells at 7 days post-irradiation and compared the expression profiles of their differentially expressed genes with senescent cells[19], revealing 17 up-regulated SASP factors(Fig5,A,C). Subsequent qRT-PCR confirmed high expression levels of IL6, IL1b, MMP1, CXCL2, and FGF2 in NHA cells after irradiation (Fig5, B). Further protein detection in conditioned medium specifically identified IL6 as the only differentially expressed SASP factor (Fig5, D). Transcriptome sequencing analysis was conducted on U251 cells treated with CM or NM (Fig5, E). The differentially expressed genes were initially filtered based on a logFC⩾1.5 and adjP < 0.05, and subsequently imported into the STRING database to construct a protein-protein interaction (PPI) network, which was then visualized using Cytoscape. Hub genes were identified using Cytohubba and CytoNCA plugins in Cytoscape. The Cytohubba plugin was used to extract the top 10 genes based on the maximum group centrality calculation method (Fig5, F). Additionally, we identified 9 genes based on a topological property analysis of betweenness centrality using CytoNCA plugin (Fig5, G). The intersection of the two methods resulted in eight differential genes (Fig5, H). Our qRT-PCR validation of eight genes showed differential expression of CSF3, CSCL3, and CCL20(Fig5, J), followed by validation of the co-enrichment pathway of the three genes (Fig5, I). The JAK2-STAT3 signaling pathway activated by IL6 was discovered. WB experiment results revealed high expression levels of p-JAK2 and p-STAT3 proteins in U251 after CM treatment (Fig5, K, L).

Discussion

Radiation induces non-neoplastic cell senescence

Radiation therapy is an indispensable treatment modality for management of the majority of cancers, and is considered the standard of care for GBM. Although intensity-modulated radiation therapy can accurately deliver radiotherapy to irregular tumor areas, minimize damage to normal brain tissue, while maximize radiation dose in tumor areas, brain damage caused by radiation is still widely recorded, and tumor recurrence is inevitable eventually[20, 21]. In addition, studies have reported that human glioma cells exhibit rapid recurrence, greater proliferation and invasion capabilities after radiotherapy[8, 9]. There are two possible explanations for this phenomenon: (1) Irradiation fails to eliminate all tumor cells; (2). Radiation may induce tumor-promoting changes in the tumor microenvironment. Cell senescence is a common alteration in tumor microenvironment after irradiation. Radiation can directly damage biological macromolecules such as DNA, proteins and lipids within cells while generating a large number of free radicals and

bioRxiv preprint doi: https://doi.org/10.1101/2024.02.21.581353; this version posted February 23, 2024. The copyright holder for this preprint (which was not certified by peer review) is the author/funder, who has granted bioRxiv a license to display the preprint in perpetuity. It is made available under aCC-BY-NC-ND 4.0 International license.

activating intracellular signaling molecules, which ultimately activities P53-P21 and p16-RB signaling pathways leading to cell cycle inhibition and a state of long-term stagnation and non-division - senescent cells[22-24]. Our study validated the occurrence of radiation-induced cell senescence, characterized by a peak in senescent cell numbers 2-7 days post-radiation followed by a gradual decline in vivo. However, in human subjects undergoing radiation therapy, the multiple exposure leads to persistent generation of senescent cells. β-galactosidase staining of tumor specimens from patients further confirmed an increased presence of senescent cells following radiation therapy.

Senescent microenvironment promotes the proliferation and invasion of GBM

The relationship between senescent cells and tumors remains uncertain. Earlier studies have demonstrated that cellular senescence can be induced by tumorigenesis itself as a protective mechanism against cancer development by preventing proliferation of mutated DNA-carrying cells[25, 26]. Senescence-associated growth arrest is perceived as an effective strategy to impede cancer progression[27]. Moreover, SASP factors can stimulate the immune surveillance mechanism and enhance the tumor suppressive function of senescent cells by directing the immune system towards generating an anticancer response[28]. However, subsequent studies have shown that SASP may exert pro-tumor effects. Inflammatory SASP factors secreted by senescent cells may inadvertently promote various aspects of tumorigenesis including cancer cell proliferation, migration, invasion, angiogenesis, epithelial-mesenchymal transition, and immune-mediated clearance[29]. In this study, a senescence microenvironment composed of senescent non-tumor cells and their secretory factors SASP was constructed by pre-irradiating cells and mouse brains to simulate the changes in tumor microenvironment induced by radiation therapy. GBM cells exhibited enhanced proliferation and invasion capabilities both in vitro and in vivo, resulting in reduced survival time for living animals. It indicates that cell senescence induced by radiotherapy can promote the rapid proliferation and invasion of residual GBM cells, and the clinical manifestation is a more aggressive disease recurrence. Navitoclax is a potent BCL-2 inhibitor with a high affinity for anti-apoptotic BCL-2 protein family (including BCL-XL, BCL-2, and BCL-w), which interferes with the interaction between pro-apoptotic and anti-apoptotic proteins of the BCL-2 family[30, 31]. It can inhibit senescent cells by blocking the anti-apoptotic proteins necessary for the survival of senescent cells. Notably, treatment with navitoclax improved intracranial tumor size and survival time in mice, providing a novel therapeutic direction for delaying GBM recurrence.

SASP promotes tumor proliferation by activating the JAK2-STAT3 signaling pathway

The mechanism underlying the promotion of GBM proliferation by senescent microenvironment remains unclear. Our findings demonstrate that the SASP factor IL6 activates the JAK2-STAT3 signaling pathway in tumor cells, leading to an up-regulation of nuclear DNA replication and

bioRxiv preprint doi: https://doi.org/10.1101/2024.02.21.581353; this version posted February 23, 2024. The copyright holder for this preprint (which was not certified by peer review) is the author/funder, who has granted bioRxiv a license to display the preprint in perpetuity. It is made available under aCC-BY-NC-ND 4.0 International license.

subsequent promotion of tumor proliferation. The JAK-STAT signaling pathway is mainly composed of cell surface receptor, JAK (janus kinase) protein family and STAT (signal transduction and activator of transcription) proteins[32]. Upon binding to the receptor, various cytokines/growth factors can phosphorylate and activate JAK, and then phosphorylate the downstream transcription factor STAT, which enters the nucleus as a dimer to regulate cell proliferation, differentiation and apoptosis[32]. JAK2-STAT3 is a major member of JAK-STAT signaling pathway and STAT3 has a potential carcinogenic effect (proto-oncogene). IL6 serves as an important ligand in the JAK2-STAT3 signaling cascade[32, 33]. Numerous studies have demonstrated that IL6 acts as a SASP factor, promoting both tumor growth and invasion[15, 34-36]. Blocking antibodies against IL6 restore tumor aggressiveness while recombinant IL-6 enhances the aggressiveness of pretumor epithelial cells co-cultured with non-senescent fibroblasts. Through mediating STAT3 activation, IL-6 drives the transcription of various MMPs that positively influence cancer aggressiveness by facilitating extracellular matrix degradation and enabling cancer cell dissemination from primary sites[34, 35]. Remarkably, among 17 senescence expression profiled SASP factors we examined in astrocyte senescence media, IL6 emerged as the most dominant one. Therefore, activation of JAK2-STAT3 signaling pathway by IL6 represents an important mechanism through which senescent cells promote GBM proliferation (Fig6).

Conclusion

The tumor microenvironment, consisting of non-neoplastic cell senescence induced by radiation therapy and its secretory phenotype, can facilitate the proliferation and invasion of GBM, indicating the favorable role of senescent cells in the recurrence of residual GBM. This process is mediated through the activation of JAK2-STAT3 signaling pathway by SASP factor IL6. Anti-senescence drugs may emerge as a novel adjunctive therapeutic approach to delay or treat GBM recurrence.

bioRxiv preprint doi: https://doi.org/10.1101/2024.02.21.581353; this version posted February 23, 2024. The copyright holder for this preprint (which was not certified by peer review) is the author/funder, who has granted bioRxiv a license to display the preprint in perpetuity. It is made available under aCC-BY-NC-ND 4.0 International license.

Ethics approval and consent to participate

All animal studies were performed under protocols approved by Experimental animal Welfare Ethics Committee, Zhongnan Hospital of Wuhan University (ZN2022179). No human trials were involved in this study.

Consent for publication

Not applicable.

Availability of data and materials

All data generated or analysed during this study are included in this published article.

Competing interests

The authors declare that they have no competing interests

Funding

This research was funded by the Excellent Doctoral Program in Zhongnan Hospital of Wuhan University (ZNYB2021015).

Authors' contributions

Pan Nie：Conceptualization, Data Curation, Formal Analysis, Investigation, Methodology, Visualization, Writing - Original Draft; Jibo Zhang and Jincao Chen:Conceptualization, Funding Acquisition, Project Administration, Resources, Supervision, Writing - Review & Editing.

Acknowledgements

We thank Zhongnan Hospital of Wuhan University for its financial assistance. We thank the Animal Experiment Center of Zhongnan Hospital of Wuhan University for raising nude mice and providing the experimental site. We would like to thank the editor and reviewers who helped to improve the article.

bioRxiv preprint doi: https://doi.org/10.1101/2024.02.21.581353; this version posted February 23, 2024. The copyright holder for this preprint (which was not certified by peer review) is the author/funder, who has granted bioRxiv a license to display the preprint in perpetuity. It is made available under aCC-BY-NC-ND 4.0 International license.

Figure Legends

Figure 1. Conditioned medium acquisition and treatments on tumor cells.

Figure 2. **(A)** β-galactosidase staining on NHA cells 7 days after radiation and mock-radiation. **(B)** mRNA expression levels of P16 and P21 genes in U251 and A172. **(C,D)** β-galactosidase staining of mouse brain tissue at different time points after radiation and trend diagram of senescent cell number. **(E)** β-galactosidase staining of human tumor specimens. Cases 1,2 and 3 were primary GBM; Cases 4,5, and 6 were recurrent GBM and received radiotherapy.

Figure 3. **(A,B)** Absorbance changes of U251 and A172 cells in different media treatment (CM or NM). **(C)** Immunofluorescence images showed ki67 protein expression in U251 cells treated with different media (CM or NM). **(D)** mRNA expression levels of ki67 gene in U251 and A172 cells treated with different media (CM or NM). **(E,F,G)** Wound healing assay. Migration rate =(initial scratch area - final scratch area)/ initial scratch area. **(H)** Transwell invasion assay.

Figure 4. **(A,C)** The enhanced CT image of the mouse brain was taken 20 days after implantation, and the image at the lower right was three-dimensional. The radiation group (Rad) had the largest tumor volume. **(B)** H&E staining of mouse brain tissue. **(D,E,F,G,H)** Kaplan-Meier survival curves of mice in different treatment groups.

Figure 5. **(A,C)** Heat map and Volcano plot of NHA senescence secretion spectrum between Rad group and Mock-Rad group. **(B)** qRT-PCR results of differential genes in senescence secretion spectrum. **(D)** The expression of senescence secretory spectrum protein in culture medium(CM or NM) was detected by ELISA. **(E)** Transcriptome sequencing differential gene volcano plot of U251 cells under different media treatment(CM or NM). **(F)** 10 genes were extracted by Cytohubba plugin based on the maximum group centrality calculation method. **(G)** 9 genes were extracted by CytoNCA plugin based on a topological property analysis of betweenness centrality. **(H)** The Venn diagram shows the intersection of the two methods. **(I)** KEGG pathway：The red circle shows the signal pathway we verified. **(J)** qRT-PCR verified the sequencing results of the differential genes. **(K)** WB: JAK2-STAT3 signal pathway. **(L)** ImageJ calculates the protein band gray value.

Figure 6. Radiation-induced senescent non-neoplastic cells secreted SASP factor IL6, which activated JAK2-STAT3 signaling pathway in tumor cells, and promoted the proliferation and invasion of GBM.

bioRxiv preprint doi: https://doi.org/10.1101/2024.02.21.581353; this version posted February 23, 2024. The copyright holder for this preprint (which was not certified by peer review) is the author/funder, who has granted bioRxiv a license to display the preprint in perpetuity. It is made available under aCC-BY-NC-ND 4.0 International license.

Reference

1. Osuka, S.,Van Meir, E.G. Overcoming therapeutic resistance in glioblastoma: the way forward. J Clin Invest. 2017;127(2):415-426.
2. Wen, P.Y.,Kesari, S. Malignant gliomas in adults. N Engl J Med. 2008;359(5):492-507.
3. Ostrom, Q.T., Cioffi, G., Gittleman, H., et al. CBTRUS Statistical Report: Primary Brain and Other Central Nervous System Tumors Diagnosed in the United States in 2012-2016. Neuro Oncol. 2019;21(Suppl 5):v1-v100.
4. Stupp, R., Mason, W.P., van den Bent, M.J., et al. Radiotherapy plus concomitant and adjuvant temozolomide for glioblastoma. N Engl J Med. 2005;352(10):987-96.
5. Wang, J.S., Wang, H.J.,Qian, H.L. Biological effects of radiation on cancer cells. Mil Med Res. 2018;5(1):20.
6. Barbagallo, G.M., Jenkinson, M.D.,Brodbelt, A.R. 'Recurrent' glioblastoma multiforme, when should we reoperate? Br J Neurosurg. 2008;22(3):452-5.
7. Seo, Y.S., Ko, I.O., Park, H., et al. Radiation-Induced Changes in Tumor Vessels and Microenvironment Contribute to Therapeutic Resistance in Glioblastoma. Front Oncol. 2019;9:1259.
8. Duan, C., Yang, R., Yuan, L., et al. Late Effects of Radiation Prime the Brain Microenvironment for Accelerated Tumor Growth. Int J Radiat Oncol Biol Phys. 2019;103(1):190-194.
9. Wang, J., Cazzato, E., Ladewig, E., et al. Clonal evolution of glioblastoma under therapy. Nat Genet. 2016;48(7):768-76.
10. Gorgoulis, V., Adams, P.D., Alimonti, A., et al. Cellular Senescence: Defining a Path Forward. Cell. 2019;179(4):813-827.
11. Hernandez-Segura, A., Nehme, J.,Demaria, M. Hallmarks of Cellular Senescence. Trends Cell Biol. 2018;28(6):436-453.
12. Lee, B.Y., Han, J.A., Im, J.S., et al. Senescence-associated beta-galactosidase is lysosomal beta-galactosidase. Aging Cell. 2006;5(2):187-95.
13. Rodier, F., Coppe, J.P., Patil, C.K., et al. Persistent DNA damage signalling triggers senescence-associated inflammatory cytokine secretion. Nat Cell Biol. 2009;11(8):973-9.
14. Zhang, R., Chen, W.,Adams, P.D. Molecular dissection of formation of senescence-associated heterochromatin foci. Mol Cell Biol. 2007;27(6):2343-58.
15. Coppe, J.P., Patil, C.K., Rodier, F., et al. Senescence-associated secretory phenotypes reveal cell-nonautonomous functions of oncogenic RAS and the p53 tumor suppressor. PLoS Biol. 2008;6(12):2853-68.
16. DeMasters, G.A., Gupta, M.S., Jones, K.R., et al. Potentiation of cell killing by fractionated radiation and suppression of proliferative recovery in MCF-7 breast tumor cells by the Vitamin D3 analog EB 1089. J Steroid Biochem Mol Biol. 2004;92(5):365-74.
17. Turnquist, C., Beck, J.A., Horikawa, I., et al. Radiation-induced astrocyte senescence is rescued by Delta133p53. Neuro Oncol. 2019;21(4):474-485.
18. Mangoni, M., Sottili, M., Gerini, C., et al. A PPAR gamma agonist protects against oral mucositis induced by irradiation in a murine model. Oral Oncol. 2017;64:52-58.
19. Coppe, J.P., Desprez, P.Y., Krtolica, A.,Campisi, J. The senescence-associated secretory phenotype: the dark side of tumor suppression. Annu Rev Pathol. 2010;5:99-118.
20. Tsien, C.I., Brown, D., Normolle, D., et al. Concurrent temozolomide and dose-escalated

bioRxiv preprint doi: https://doi.org/10.1101/2024.02.21.581353; this version posted February 23, 2024. The copyright holder for this preprint (which was not certified by peer review) is the author/funder, who has granted bioRxiv a license to display the preprint in perpetuity. It is made available under aCC-BY-NC-ND 4.0 International license.

intensity-modulated radiation therapy in newly diagnosed glioblastoma. Clin Cancer Res. 2012;18(1):273-9.

21. Zhuang, H., Shi, S., Yuan, Z.,Chang, J.Y. Bevacizumab treatment for radiation brain necrosis: mechanism, efficacy and issues. Mol Cancer. 2019;18(1):21.
22. Chen, L., Yang, R., Qiao, W., et al. 1,25-Dihydroxyvitamin D exerts an antiaging role by activation of Nrf2-antioxidant signaling and inactivation of p16/p53-senescence signaling. Aging Cell. 2019;18(3):e12951.
23. Gimenez-Bastida, J.A., Avila-Galvez, M.A., Espin, J.C.,Gonzalez-Sarrias, A. Conjugated Physiological Resveratrol Metabolites Induce Senescence in Breast Cancer Cells: Role of p53/p21 and p16/Rb Pathways, and ABC Transporters. Mol Nutr Food Res. 2019;63(22):e1900629.
24. Sanders, J.T., Freeman, T.F., Xu, Y., et al. Radiation-induced DNA damage and repair effects on 3D genome organization. Nat Commun. 2020;11(1):6178.
25. Serrano, M., Lin, A.W., McCurrach, M.E., Beach, D.,Lowe, S.W. Oncogenic ras provokes premature cell senescence associated with accumulation of p53 and p16INK4a. Cell. 1997;88(5):593-602.
26. Xu, M., Pirtskhalava, T., Farr, J.N., et al. Senolytics improve physical function and increase lifespan in old age. Nat Med. 2018;24(8):1246-1256.
27. Collado, M., Gil, J., Efeyan, A., et al. Tumour biology: senescence in premalignant tumours. Nature. 2005;436(7051):642.
28. Ewald, J.A., Desotelle, J.A., Wilding, G.,Jarrard, D.F. Therapy-induced senescence in cancer. J Natl Cancer Inst. 2010;102(20):1536-46.
29. Wang, B., Kohli, J.,Demaria, M. Senescent Cells in Cancer Therapy: Friends or Foes? Trends Cancer. 2020;6(10):838-857.
30. Chang, J., Wang, Y., Shao, L., et al. Clearance of senescent cells by ABT263 rejuvenates aged hematopoietic stem cells in mice. Nat Med. 2016;22(1):78-83.
31. Saleh, T., Carpenter, V.J., Tyutyunyk-Massey, L., et al. Clearance of therapy-induced senescent tumor cells by the senolytic ABT-263 via interference with BCL-X(L) -BAX interaction. Mol Oncol. 2020;14(10):2504-2519.
32. Hu, X., Li, J., Fu, M., Zhao, X.,Wang, W. The JAK/STAT signaling pathway: from bench to clinic. Signal Transduct Target Ther. 2021;6(1):402.
33. Huang, B., Lang, X.,Li, X. The role of IL-6/JAK2/STAT3 signaling pathway in cancers. Front Oncol. 2022;12:1023177.
34. Fisher, D.T., Appenheimer, M.M.,Evans, S.S. The two faces of IL-6 in the tumor microenvironment. Semin Immunol. 2014;26(1):38-47.
35. Kessenbrock, K., Plaks, V.,Werb, Z. Matrix metalloproteinases: regulators of the tumor microenvironment. Cell. 2010;141(1):52-67.
36. Miao, J.W., Liu, L.J.,Huang, J. Interleukin-6-induced epithelial-mesenchymal transition through signal transducer and activator of transcription 3 in human cervical carcinoma. Int J Oncol. 2014;45(1):165-76.

Table1
bioRxiv preprint doi: https://doi.org/10.1101/2024.02.21.581353; this version posted February 23, 2024. The copyright holder for this preprint (which was not certified by peer review) is the author/funder, who has granted bioRxiv a license to display the preprint in perpetuity. It is made available under aCC-BY-NC-ND 4.0 International license.
Click here to access/download Table Table1.docx

Table 1 The tumor volume and survival time of mice

	Tumor volme in 20th day after implantation（mm^3）	Survival time after implantation（days）
Control group	26.8±14.2	26.7±3.1
RAD group	76.0±31.4	22.3±1.7
RAD＆dose group	38.3±16.5	27.1±3.3
Dose group	24.4±14.0	28.7±4.5

Notes: RAD: Radiation.

Dose: Anti-senescence drug, navitoclax.

Figure1

Click here to access/download;Figure;Fig1.tif

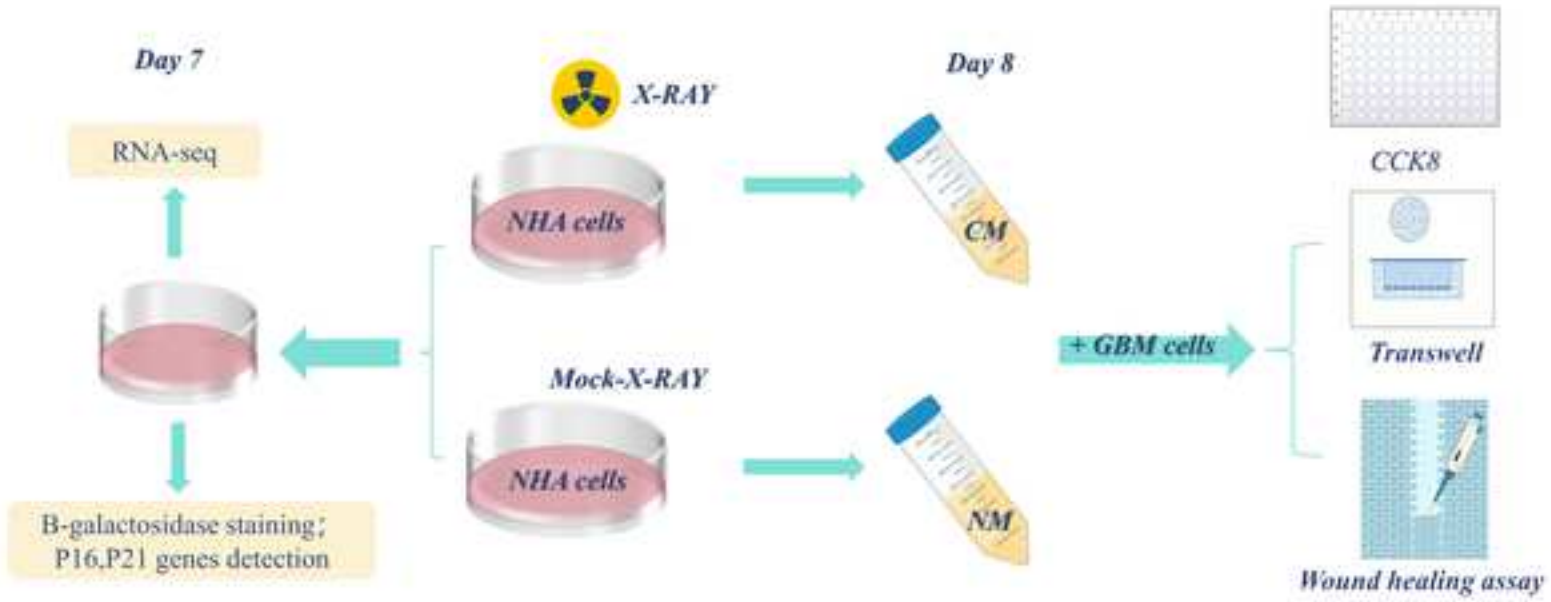

Figure2

Click here to access/download;Figure;Fig2.tif

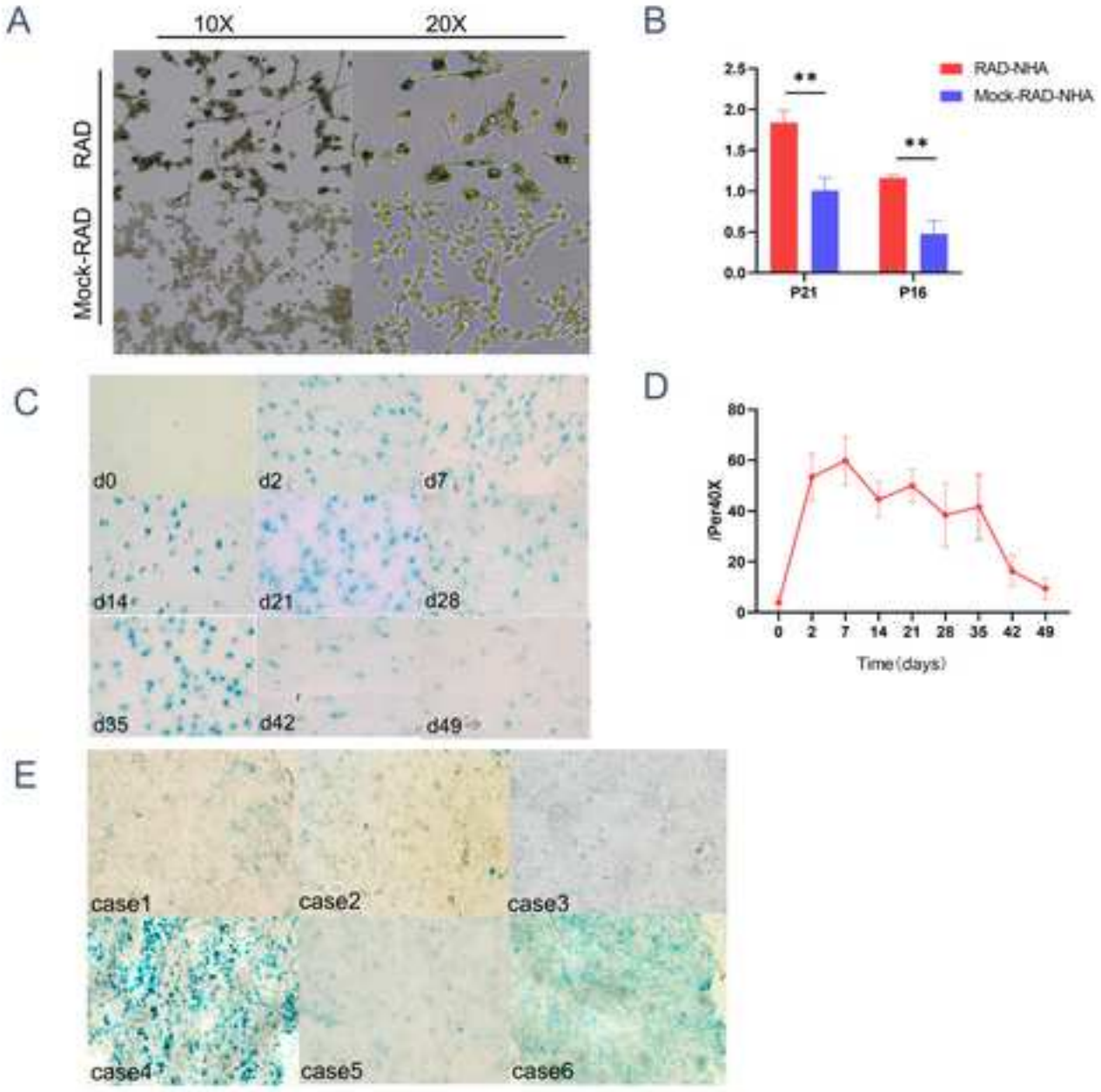

Figure3

Click here to access/download;Figure;Fig3.tif

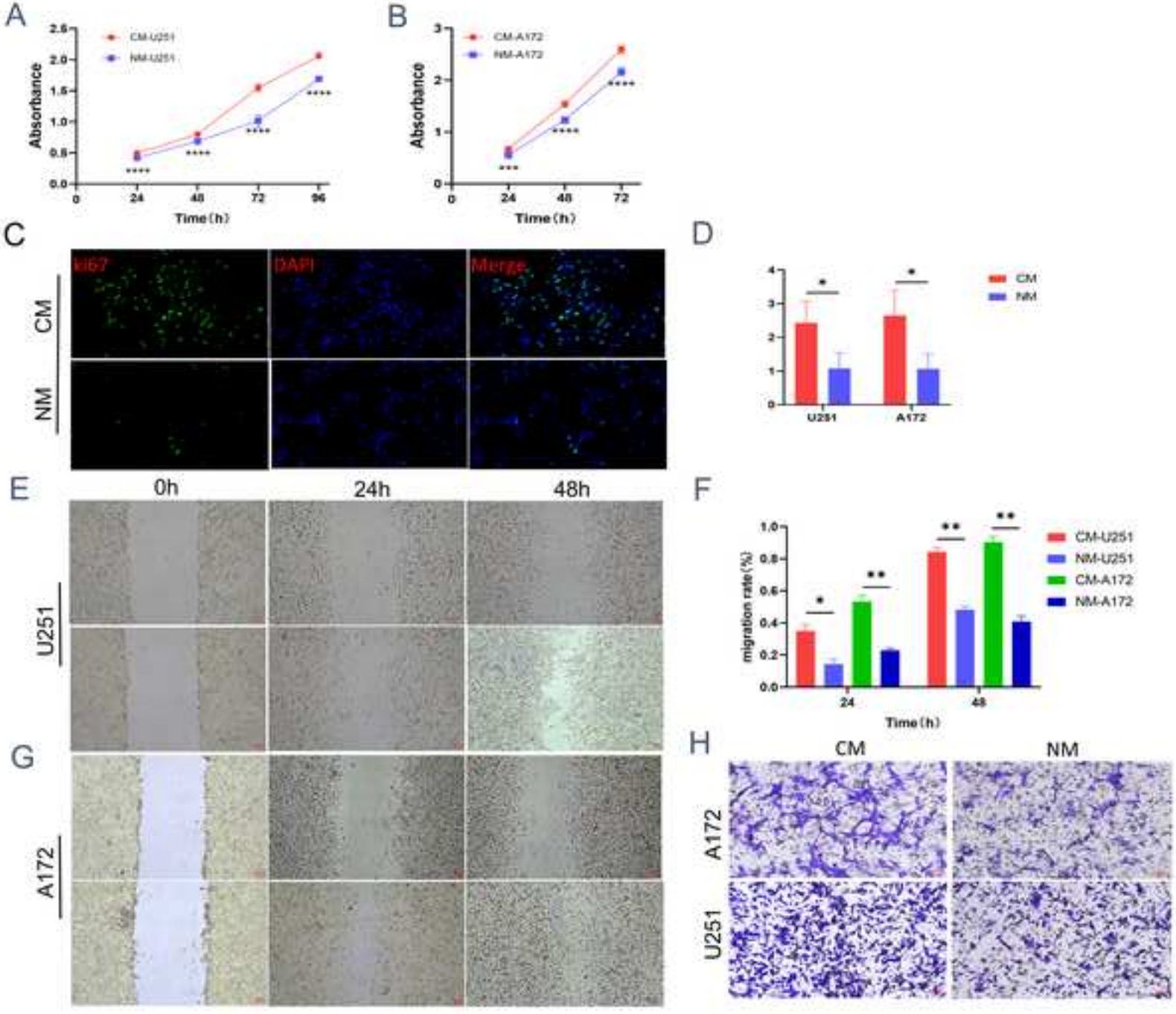

Figure4

Click here to access/download;Figure;Fig4.tif

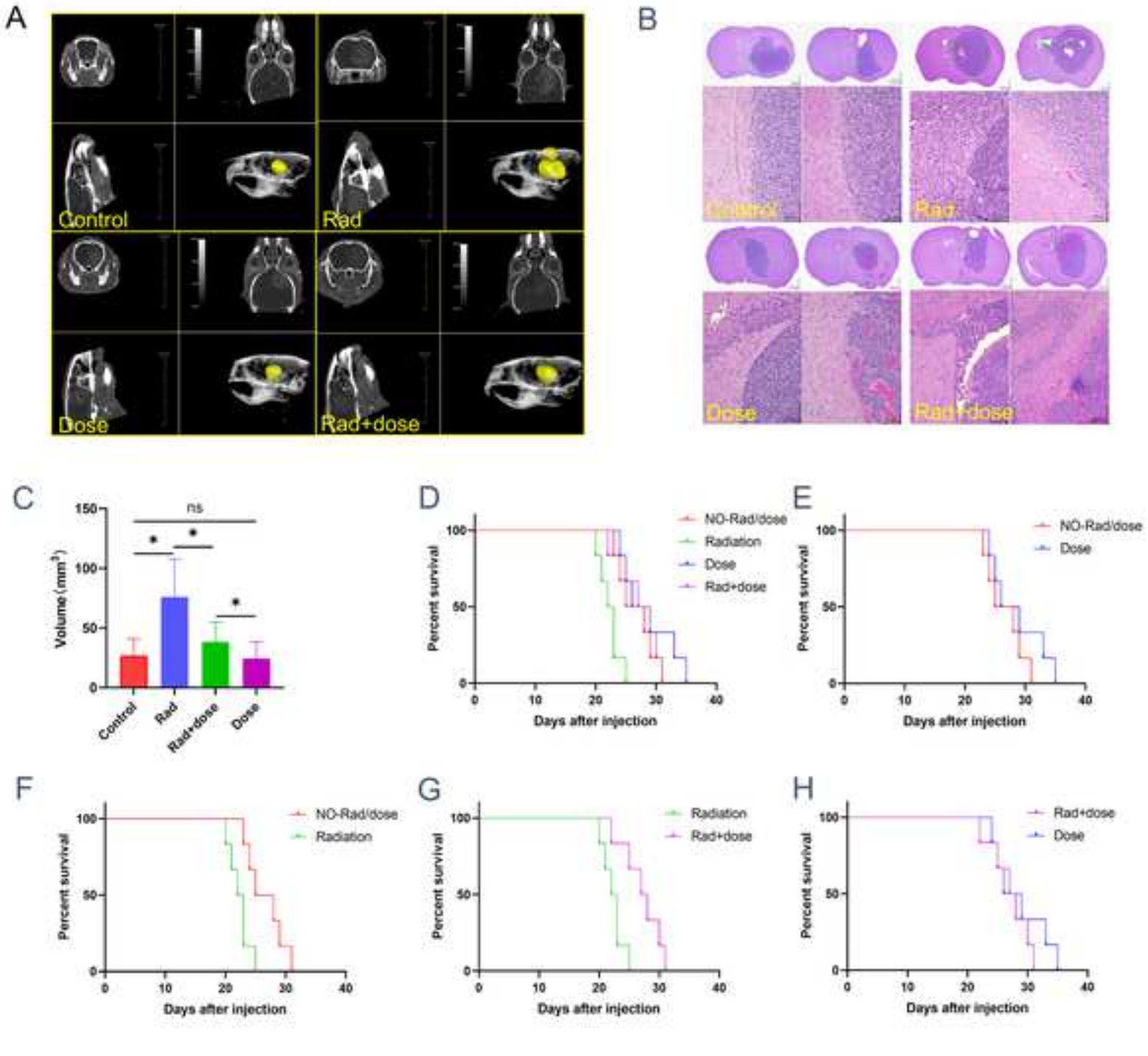

Figure5

Click here to access/download;Figure;Fig5.tif

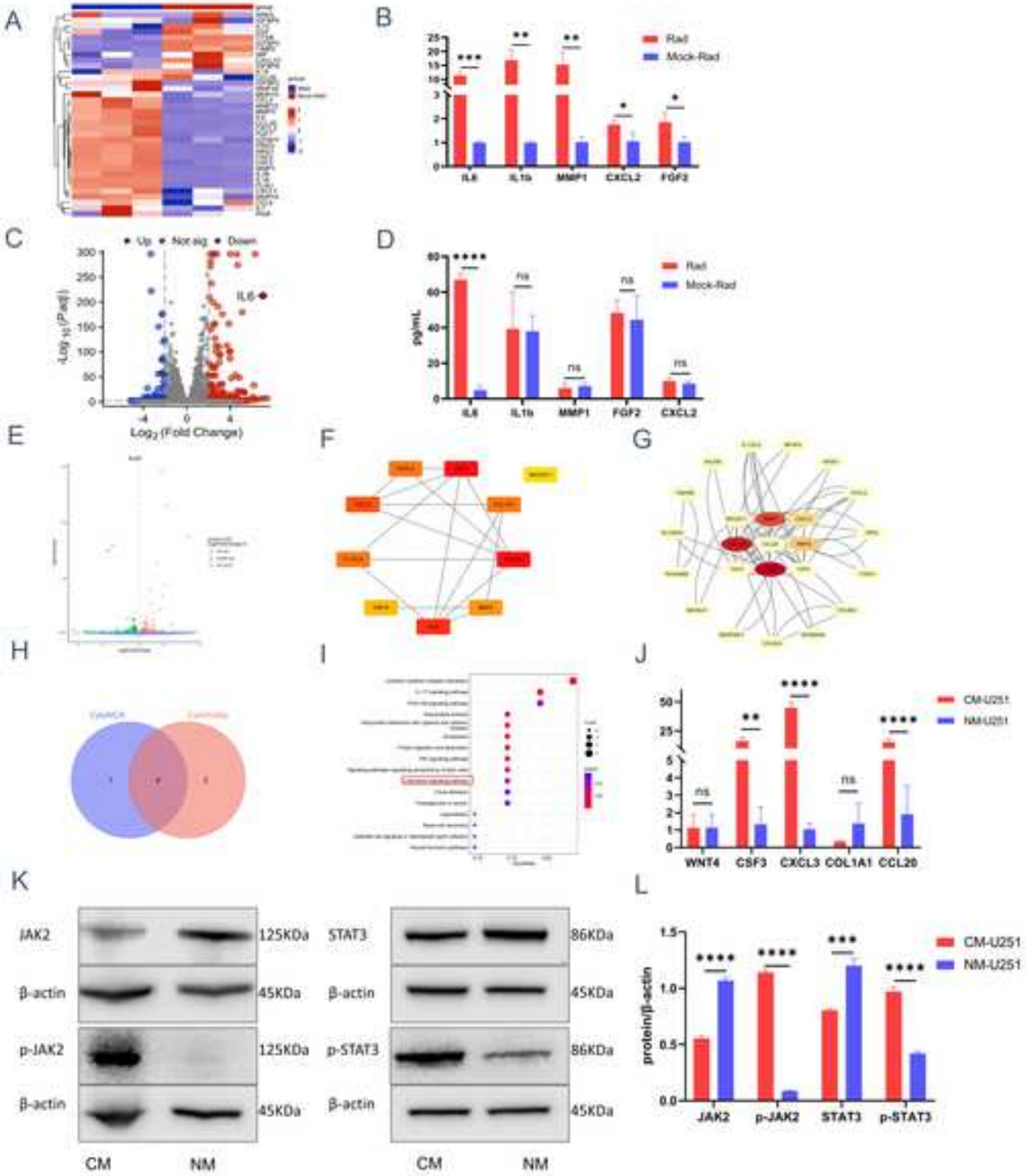

Figure6

Click here to access/download;Figure;Fig6.tif